Liquid phase structure within an unsaturated fracture network beneath a surface infiltration event: Field experiment

Robert J. Glass

Flow Visualization and Processes Laboratory, Sandia National Laboratories, Albuquerque, New Mexico, USA

Michael J. Nicholl

Department of Materials, Metallurgical, Mining and Geological Engineering, University of Idaho, Moscow, Idaho, USA

Abelardo L. Ramirez and William D. Daily

Lawrence Livermore National Laboratory, Livermore, California, USA

Received 27 December 2000; revised 25 October 2001; accepted 4 February 2002; published 18 October 2002.

[1] We conducted a simple field experiment to elucidate structure (i.e., geometry) of the liquid phase (water) resulting from ponded infiltration into a pervasive fracture network that dissected a nearly impermeable rock matrix. Over a 46 min period, dyed water was infiltrated from a surface pond while electrical resistance tomography (ERT) was employed to monitor the rapid invasion of the initially dry fracture network and subsequent drainage. We then excavated the rock mass to a depth of ~5 m, mapping the fracture network and extent of dye staining over a series of horizontal pavements located directly beneath the pond. Near the infiltration surface, flow was dominated by viscous forces, and the fracture network was fully stained. With increasing depth, flow transitioned to unsaturated conditions, and the phase structure became complicated, exhibiting evidence of fragmentation, preferential flow, fingers, irregular wetting patterns, and varied behavior at fracture intersections. ERT images demonstrate that water spanned the instrumented network rapidly on ponding and also rapidly drained after ponding was terminated. Estimates suggest that our excavation captured from ~15 to 1% or less of the rock volume interrogated by our infiltration slug, and thus the penetration depth from our short ponding event could have been quite large. *INDEX TERMS:* 1875 Hydrology: Unsaturated zone; 1829 Hydrology: Groundwater hydrology; 1832 Hydrology: Groundwater transport; *KEYWORDS:* fractures, fractured rock, unsaturated flow, infiltration, preferential flow

Citation: Glass, R. J., M. J. Nicholl, A. L. Ramirez, and W. D. Daily, Liquid phase structure within an unsaturated fracture network beneath a surface infiltration event: Field experiment, *Water Resour. Res.*, *38*(10), 1199, doi:10.1029/2000WR000167, 2002.

1. Introduction

[2] In recent years, a significant body of research has considered flow and transport in unsaturated fractured rock within arid environments. Early conceptual models [e.g., *Wang and Narasimhan*, 1985, 1993; *Pruess and Wang*, 1987; *Peters and Klavetter*, 1988] have been called into question by both laboratory experiments focused on basic processes [e.g., *Glass et al.*, 1995, 1996; *Tokunaga and Wan*, 1997] and field evidence that indicates rapid deep percolation in arid environments [e.g., *Russell et al.*, 1987; *Fabryka-Martin et al.*, 1996; *Yang et al.*, 1996; *Davidson et al.*, 1998]. Calculational models have been proposed to fix some of these conceptual model failures; however, such models typically rely on calibrated approaches, and hence are unable to provide better understanding of system behavior [e.g., *Liu et al.*, 1998]. While laboratory experiments greatly increase our fundamental understanding of physical processes, field experiments contain a much higher level of ambiguity, as measurements are difficult to make and interpret [e.g., *Kilbury et al.*, 1986; *Drier et al.*, 1987; *Gimmi et al.*, 1997; *Dahan et al.*, 1999; *Bussod et al.*, 1999; *Faybishenko et al.*, 2000].

[3] Conceptualization of flow and transport within an unsaturated fractured rock mass requires an understanding of how the geometry, or structure, of the water/air phases evolves in time. In addition to defining transport pathways for water and solutes, this structure also sets the domain for interactions between the phases (air/liquid/solid). Full treatment of this problem requires that we consider phase structure within the entire void space (fracture and matrix). We can think of the relative importance of fractures and matrix within the void space as spanning a spectrum of possibility. At one end of the spectrum, properties of each are identical, and fractures become indistinguishable from the matrix; at the other end, permeable fractures are imbedded in an impermeable rock matrix, giving the fractures full control over flow and transport. Superimposed on this first order spectrum are a host of coupled biogeochemical, geomechanical, and hydrologic processes that can modify the void space and its surface chemistry in time. The surfaces of fractures are subject to alteration due to: mineralogic weathering, erosion [e.g., *Weisbrod et al.*, 1998, 1999, 2000a],

0043-1397/02/2000WR000167$09.00

deposition/dissolution [e.g., *Bekri et al.*, 1997; *Hanna and Rajaram*, 1998; *Weisbrod et al.*, 2000b], and biofilm development [e.g., *Brown et al.*, 1994]; furthermore, geometry of the entire network may shift with temporal changes in the stress field [e.g., *National Research Council*, 1996]. Whatever the void space or surface chemistry within an unsaturated fractured rock mass, phase structure within that void space will control flow and transport.

[4] Understanding phase structure in fractured rock begins by considering the simplest system of a single fracture within an impermeable matrix in the absence of geochemical, biological, or geomechanical complications. Research in laboratory systems of this nature has been reviewed in the context of two-phase flow [*National Research Council*, 1996]; and more recently, used to develop computational models at the single fracture scale [*Glass et al.*, 2001]. Under low flow conditions, where viscous forces are small relative to capillary or gravity forces, laboratory experiments and numerical simulations have shown that the physics of fluid–fluid displacement can lead to intricate phase structure that exhibits complicated dynamic behavior. These structures include gravity driven fingers [e.g., *Nicholl et al.*, 1992, 1993a, 1993b, 1994; *Glass*, 1993; *Su et al.*, 1999], intricate and ramified gas phase entrapment [e.g., *Glass*, 1993; *Nicholl and Glass*, 1994; *Glass and Nicholl*, 1995a, 1995b; *Glass et al.*, 1998], and intermittent/chaotic pulsation [e.g., *Nicholl et al.*, 1993a; *Glass and Nicholl*, 1996; *Su et al.*, 1999]. In each case, phase structure may span the fracture aperture while wetting only a small portion of the fracture surfaces. At higher flow rates, viscous forces increase, capillary/gravity induced effects decrease, and structure of the wetting phase within the fracture becomes pervasive [e.g., *Nicholl et al.*, 1992, 1993a; *Nicholl and Glass*, 1994]. More recently, it has also been found that under certain pressure regimes, nonaperture spanning water film flow within the roughness of the rock surfaces can define an additional conductive structure [e.g., *Tokunaga and Wan*, 1997, 2001a, 2001b; *Or and Tuller*, 2000].

[5] Such understanding gained at the single fracture scale suggests that individual fractures and fracture intersections will place a critical control on flow in fracture-matrix networks by acting as capillary barriers and flow integrators. As a result, properly including the influence of discrete fractures is expected to yield behavior that is fundamentally at odds with currently accepted conceptual models for flow through unsaturated fractured rock [see *Glass et al.*, 1995, 1996]. If we take additional steps toward general field settings and superimpose processes that can lead to temporal changes in void space geometry [*Weisbrod et al.*, 1998, 1999, 2000a, 2000b; *Bekri et al.*, 1997; *Hanna and Rajaram*, 1998; *Brown et al.*, 1994], interphase properties such as contact angle and interfacial tension [e.g., *Totsche et al.*, 1997], and boundary/initial conditions defined by the weather, we must admit that our ability to predict flow and transport in unsaturated fractured rock is at present truly limited.

[6] To appropriately consider the growth and dynamics of phase structure within fracture networks, experiments are required where we can systematically vary the relative importance of capillary, gravity, and viscous forces within a controlled fracture network topology. Such experiments must be designed so that they can consider the influence of initial/boundary conditions as well as slight shifts in the relative importance of the local forces with time and space due to additional factors such as stress fields, chemistry, biology, or particulate transport and filtering. In the formative stages of such an effort, guidance from field experiments is highly desirable, even though interpretation and generalization of site-specific results is always difficult. In 1994, an opportunity arose to conduct a simple field experiment that would explore liquid phase structure resulting from a surface ponding event in an initially dry fracture network. Construction of a test facility at the Nevada Test Site (NTS) required the excavation of a large, pervasively fractured rock mass having hydraulic properties that precluded significant matrix interaction. Prior to excavation, we infiltrated a water slug containing a visible tracer into the rock unit and used Electrical Resistance Tomography (ERT) to follow the gross evolution of the phase structure during infiltration and subsequent drainage. Then, during site excavation, we mapped the fracture network and tracer distribution within a series of horizontal pavements immediately below the infiltration surface. In the following, we present the critical aspects of our test, along with the first description of phase structure within an unsaturated, natural fracture network.

2. Experimental Investigation

[7] Our experiment was performed adjacent to the Large Block Test (LBT), a scientific investigation conducted by Lawrence Livermore National Laboratory on the eastern slope of Fran Ridge, near Yucca Mountain, Nevada [see *Lin et al.*, 1994, 2001; *Wilder et al.*, 1997; *Ramirez and Daily*, 2001]. The LBT was sited at the base of Fran Ridge in order to access an outcrop of nonlithophysal Topopah Spring welded tuff; a stratigraphic unit being considered as a potential host for disposal of high-level radioactive waste. Preparations for the LBT included carefully removing the rock surrounding a large ($4.5 \times 3 \times 3$ m) block of Topopah Spring tuff; opportunistically, we designed our test to make use of the scheduled excavation process. Our principle objective was to map the fracture network and liquid structure beneath an infiltration event. A secondary objective was to capture gross dynamics of phase structure development within the network, during both infiltration and subsequent drainage. To accomplish these objectives, we selected a location adjacent to that chosen for the LBT, infiltrated dyed water into the rock mass, and followed it with Electrical Resistance Tomography (ERT); later, as excavation for the LBT continued, we mapped the fracture network and dye structure beneath our infiltration site. We chose a ponded source because it: (1) mimicked a far from equilibrium, possibly deep penetration, high flow situation as may occur during a thunderstorm; (2) was most easily implemented in the very short timeframe allowed for the test; and (3) would give the best conditions for ERT to visualize water within the fractured rock mass. In this section, we present a concise description of site preparation, infiltration event, ERT application, excavation, and mapping; further details, a complete set of all data, and numerous photographs documenting these activities are given by *Nicholl and Glass* [2002].

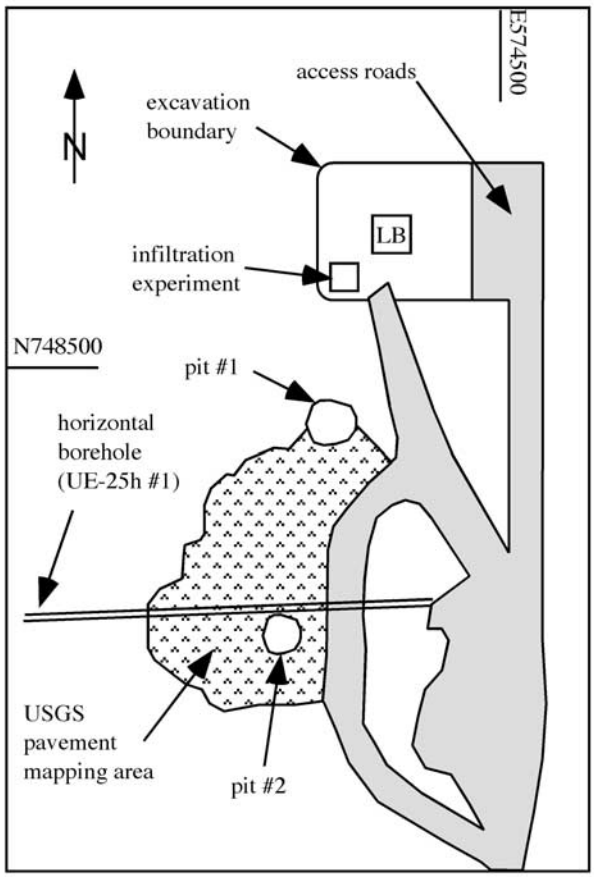

Figure 1. Sketch of the general site layout. Drawing shows the location of various site activities and is not to scale [after *Lin et al.*, 1994]. Yucca Mountain is located directly to the west, and 40 Mile Wash is to the east. Our infiltration experiment was performed in the region excavated to prepare for the Large Block Test (LBT). Fractures exposed on the pavement area and in pits to the south and west of the excavation are described by *Throckmorton and Verbeek* [1995].

[8] Prior to our infiltration test, a level work area (~15 × 15 m) was excavated to a depth of ~1–3 m below ground surface, and the LBT block was isolated from the formation with ~5 m deep vertical saw cuts. We selected an ~6 m^2 (8 × 8′) site in the southwest corner of the leveled area (Figure 1) for our test. Visual inspection of the excavation pavement and walls at this location suggested that the extremely tight matrix of this densely welded unit would confine the majority of flow to the pervasive (<30 cm spacing) fracture network. Exposed fractures also showed relatively small amounts of secondary mineralization (e.g., coating, filling). The infiltration site was prepared by excavating a shallow (~0.2 m) depression for the pond (~3.5 m^2 surface area, see Figure 2) into the rock surface and installing the ERT array (described below).

[9] Initial conditions for the near surface fracture network were very dry, significant rainfall had not occurred for some months, and potential evapotranspiration in this region (125–200+ cm/yr) greatly exceeds annual rainfall (8–10 cm/yr) [*Bedinger et al.*, 1990]. Approximately 800 L of infiltration liquid were prepared by adding 4 g/L of blue food coloring (FD&C Blue #1) to local well water. We chose food coloring because it is nontoxic, highly visible, and readily adsorbed onto the fracture surfaces. The infiltration test was initiated by pouring 150 L of liquid into the pond from buckets. At the same time, gravity flow was induced from a feed tank located several meters above the infiltration pond (Figure 3). Pond level was stabilized ~10 min after initiating flow; afterward, we measured steady infiltration (0.26 L/s) until the feed tanks were depleted at 36 min (Figure 4). Water depth within the pond varied according to the rough nature of the excavated surface, with a range of from ~2.5 to ~15 cm and average of ~4 cm. After the feed tanks were depleted, nearly all of remaining pond disappeared into the fracture network over the next ~10 min, fragmenting the pool into a number of small puddles on the irregular surface. In all, we added 790 L of water to the pond (150 L poured from the buckets to start the experiment and 640 L added from the feed tanks); a negligible amount was trapped in small depressions and did not infiltrate into the fracture network.

[10] An ERT array was installed to measure resistivity over a set of two-dimensional vertical planes beneath the infiltration surface; measurements were taken before, during, and after ponding, with the expectation that changes in moisture content within the fracture network would produce a measurable change in resistivity. Four ERT strings (designated 1 through 4), each 3 m long and containing 11 electrodes (30 cm apart) were grouted into dry drilled vertical holes located within the pond at the corners of a 1.06 × 1.06 m square (see Figure 2). Installation was

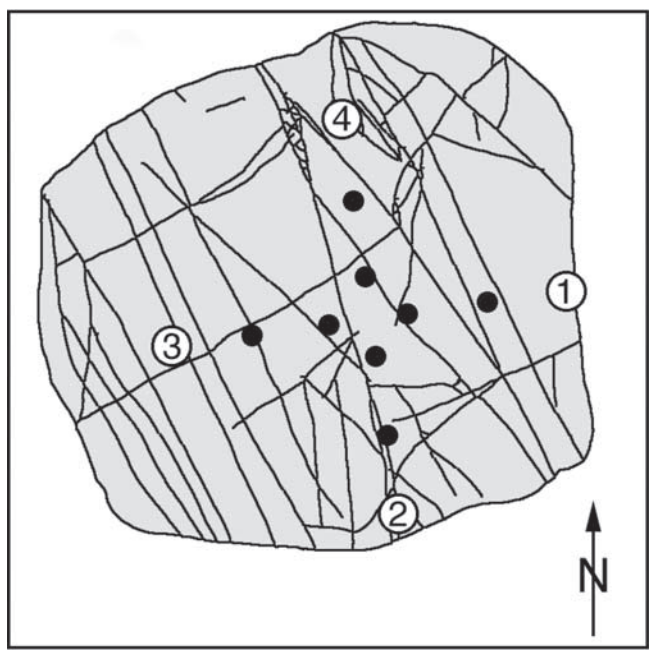

Figure 2. Infiltration pond and ERT array. Area excavated for the pond is shown in gray. The box surrounding the pond shows the ~6 m^2 (8 × 8′) mapping region; at this elevation, fractures outside the pond were not mapped. Numbered circles depict location of the primary ERT strings, and solid circles represent the surface electrodes.

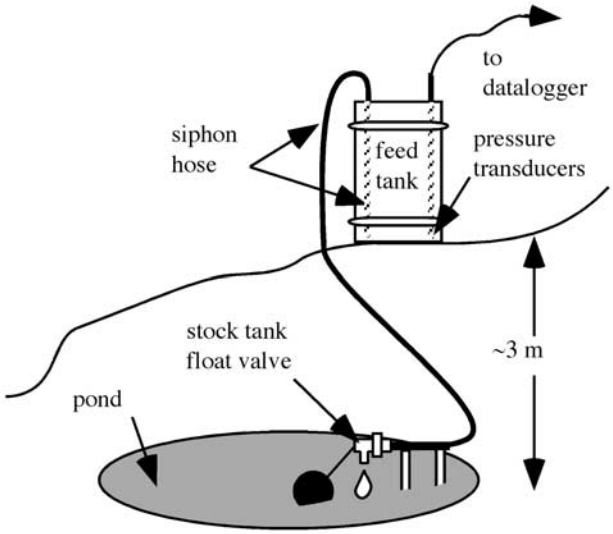

Figure 3. Sketch of the infiltration pond and apparatus. Note that the actual pond was neither round (see Figure 2) nor was the bottom flat. Constant water level in the pond was maintained with a float valve designed for use in stock tanks. A drop in pond level would open the float valve and induce gravity flow from a feed tank located on the adjacent hillside. Outflow rate from the feed tank was obtained by measuring liquid depth in the tank at 10 s intervals with a pair of calibrated pressure transducers read by a data logger.

designed to minimize perturbations to the system, provide electrical contact with the rock mass, inhibit the formation of preferential pathways, and maximize coverage across the primary vertical fracture sets. Eight shallow (15 cm) surface electrodes were installed along diagonals of the square (30 cm apart) to increase resolution in those planes. A full suite of measurements (i.e., all linearly independent transfer resistances were collected using a 4 pole measurement approach) was taken on the day before and after the test. Because of the short duration of the ponding event and the ~22 min period required to complete a survey of a single plane, measurements during ponding and shortly thereafter were limited to the sequence: 1–3 plane (2–24 min), 1–3 plane (24–44 min), 2–4 plane (52–74 min), 1–3 plane (77–99 min), ending with the 2–4 plane (114–136 min).

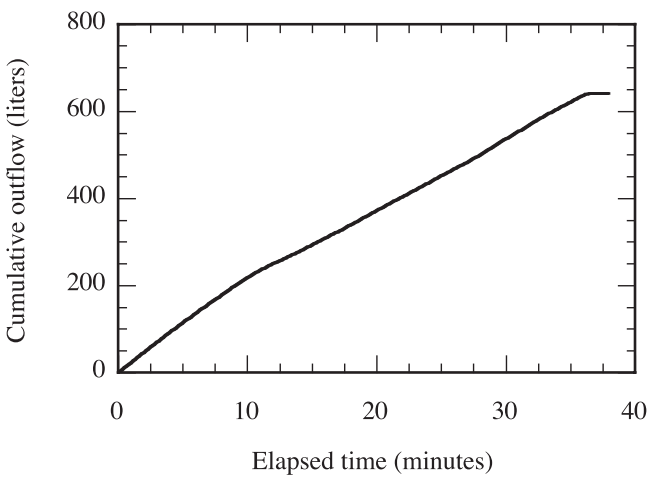

Figure 4. Cumulative outflow in time. After setting the float valve in the pond ~10 min into the test, outflow from the feed tank yields infiltration (0.26 L/s), which remained relatively steady until fluid addition was stopped at 36 min.

[11] Removal of rock surrounding the LBT block (including the region of our test) began approximately eight weeks after the infiltration event, and lasted for a 3 month period. The delay provided sufficient time for water held in near surface fractures to either evaporate or imbibe into the surrounding matrix. Rock surrounding the LBT was removed in a series of roughly horizontal lifts. At each level, the exposed rock pavement was broken to a depth of ~0.5 m with a large vehicle-mounted jackhammer (~0.5 m chisel) and most of the waste rock was removed with a small bulldozer. The pavement was then cleaned to bare rock over a ~6 m^2 ($8 \times 8'$) area directly below the infiltration site. Large rocks were moved by hand, and fine debris was blown away with pressurized air. The fracture network and distribution of tracer were mapped at the infiltration surface (level 0), and at each of the eleven subsequent excavation levels (1–11). Maps were referenced to a portable 2.44 × 2.44 m ($8 \times 8'$) grid that was subdivided at 0.305 × 0.305 m ($1 \times 1'$) intervals. Fracture traces and dye stains were recorded at a scale of $1'' = 1'$ by hand mapping (see Figure 5 for a scanned and interpreted

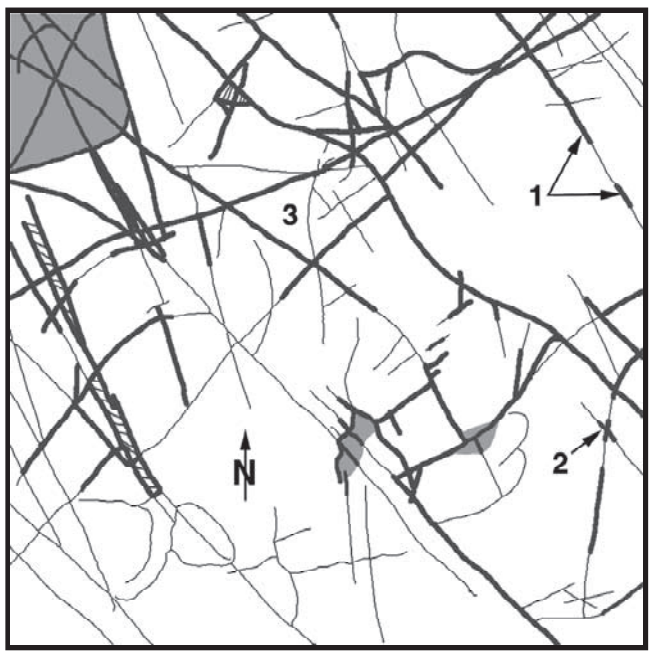

Figure 5. Example detailed pavement map at level 8. For clarity, the hand-drawn map of the $8' \times 8'$ region has been redrafted to focus on the spatial distribution of stained and unstained fractures; a full set of original maps, which include fracture dip and other ancillary information, is given by *Nicholl and Glass* [2002]. Unstained fractures are shown as thin black lines, stained fractures are shown as thick dark gray lines, and areas of pervasive stain on subhorizontal fractures are shown in light gray. Within this map, one can see a number of small-scale flow features: (1) fragmented flow along a single fracture; (2) concentration of flow at fracture intersections; and (3) bypassing of fractures, despite obvious physical connection to the flow field.

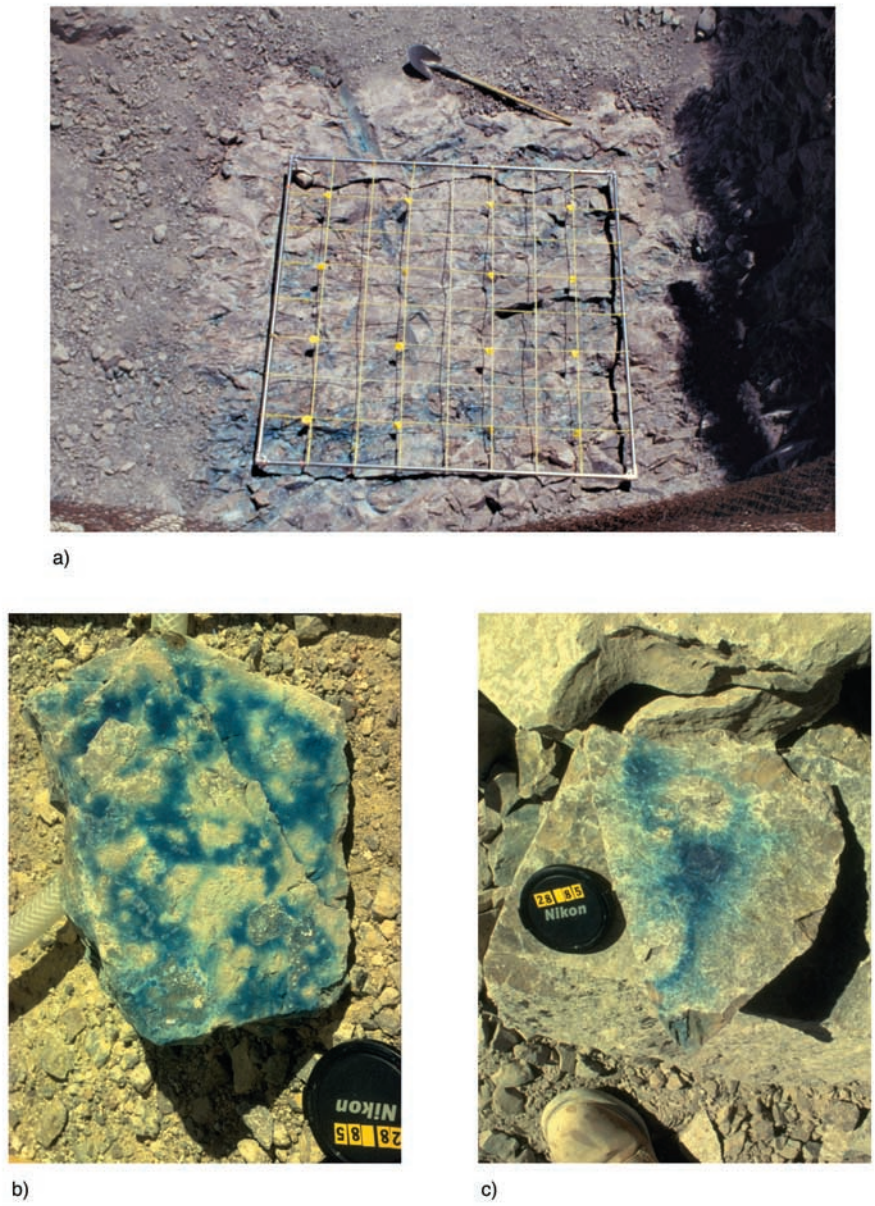

Figure 6. Photographs. (a) View looking eastward and down onto the mapped area at a depth of ~2.5 m below the infiltration surface (level 6). Tracer stain is clearly concentrated in the northwest corner of the mapped area (lower left corner of the grid) and extends outward in that direction. A steeply dipping fracture exiting the mapped area to the northeast (left of the shovel) shows stain extending away from the mapped area. A 1 m wide buffer zone surrounding the LBT can be seen protruding into the upper left of the photograph. Wire mesh in the foreground was draped over the excavation wall to protect against rockfall. (b) Complicated flow structure within the plane of a single fracture; lens cap is shown for scale. Sample was found within the excavated rubble at a depth of 3–4 m below the infiltration surface; however, the horizontal location is not known. Tracer appears to be connected in all directions, suggesting capillary dominated flow. Large portions of the aperture field were apparently bypassed by the invading liquid. (c) Evidence of preferential flow along a fracture plane; lens cap is shown for scale. Sample was found within the excavated rubble at a depth of 3–4 m below the infiltration surface; however, the horizontal location is not known. Flow structure spans the fracture in only one direction, suggestive of a gravity-driven finger.

example map). The longest fracture traces were mapped first, and then successively smaller features as time allowed. Wherever possible, the dip of individual fractures was measured (±5°) on exposed surfaces. At each level, 35 mm slides were taken across the grid to capture interesting structure (dye and fractures) as were perspective views (see example in Figure 6). During excavation, we also noted the approximate location and extent of tracer encountered out-

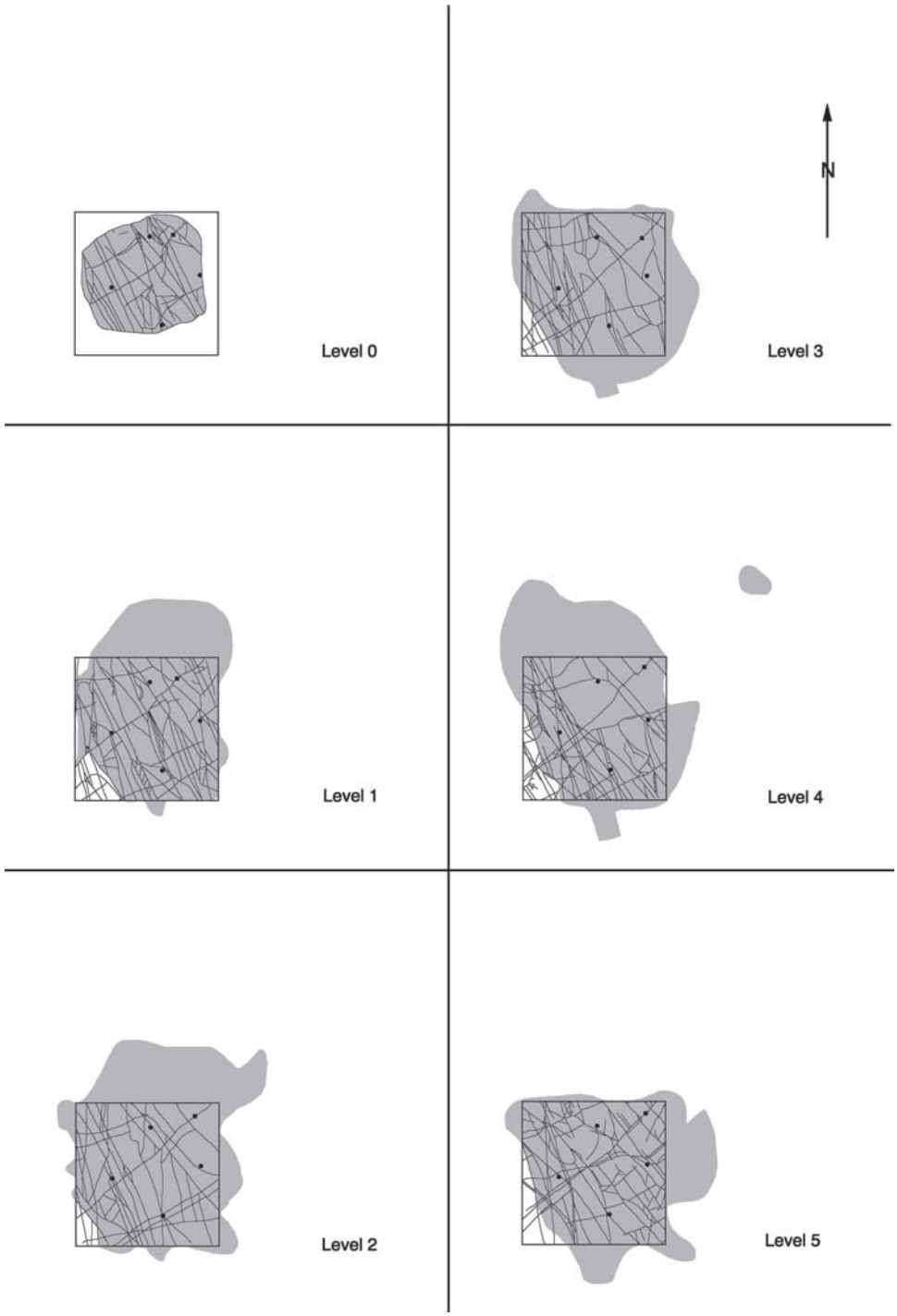

Figure 7. Fracture maps and observations of gross dye presence, levels 0 through 11. Areas in which fractures containing tracer were observed are shown in gray. Level 0 is the infiltration surface, where mapping was limited to areas within the infiltration pond. At each level, the $\sim$6 m^2 ($8 \times 8'$) detailed mapping region is outlined; estimates of tracer location outside that region are based on 35 mm slides and notes taken during the excavation process. The four primary ERT strings did not extend to the bottom of the excavation and are marked as solid circles on the maps for levels 1–7; numbering convention for the ERT strings is shown in Figure 2. A persistent near-vertical fracture trending SW–NE is marked with a black square.

side of the mapped area (e.g., on fractures in the excavation walls and in the excavated rubble).

[12] Finally, we note that the excavation process was designed specifically for the LBT investigation and placed some constraints on our mapping process: (1) Vertical interval between pavements was not consistent. (2) Roughness and dip of the mapped area varied considerably. (3) Only a small area was cleared to bare rock, hence we were

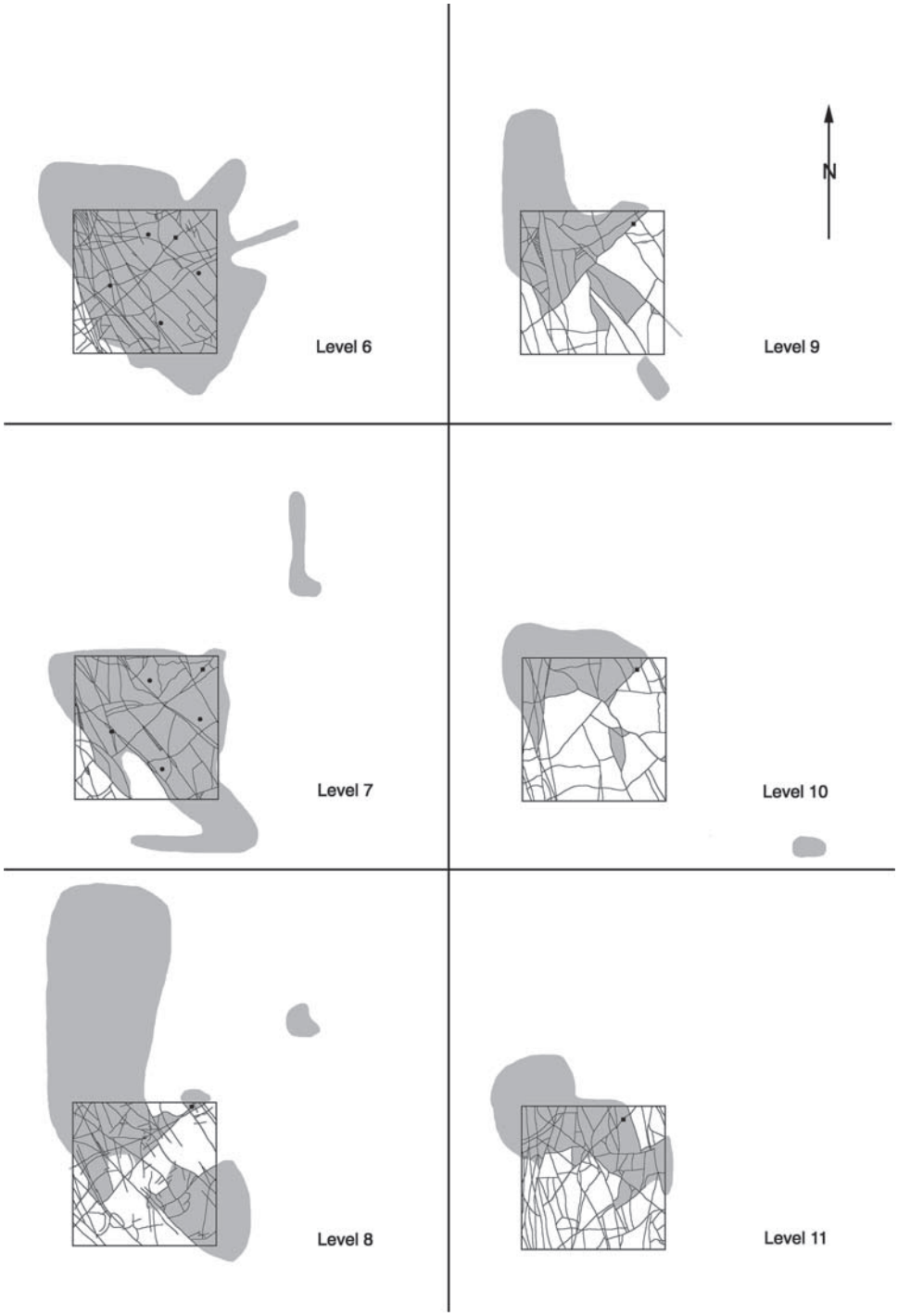

Figure 7. (continued)

unable to obtain a detailed record of tracer migration outside of the mapped area. (4) Excavation was restricted to horizontal pavements; therefore we could not explore evidence of flow mechanisms in the plane of inclined fractures (e.g., gravity driven fingering) except through observation of broken blocks. (5) Mapping activities were performed immediately after a lift was cleaned, and sometimes the excavation schedule limited the time available. As a result, maps taken at levels 7, 9, and 10 contain less detail than those at other levels. (6) Excavation stopped at a depth of $\sim$5 m, while the infiltration pulse clearly penetrated to additional depth.

3. Results and Interpretation

[13] Fracture maps combined with observations of gross dye presence (inside and outside the mapped region) for all levels are shown in Figure 7; gray regions on the maps denote the domain in which tracer was observed. A comparison between Figures 5 and 7, level 8, elucidates the

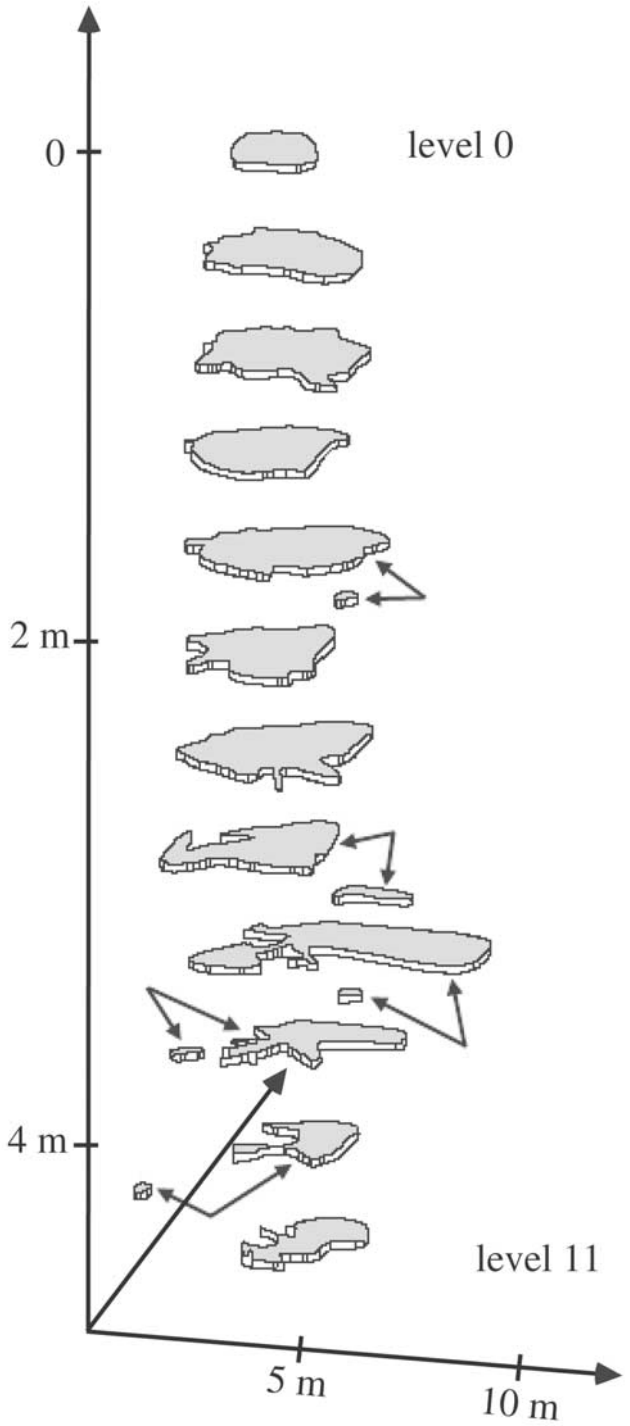

Figure 8. Three-dimensional perspective of the tracer extent. Gray zones in Figure 7 that represent tracer extent at each excavated level have been stacked to illustrate lateral variability in the flow field with depth. This diagram has been significantly expanded in the vertical direction to facilitate discrimination between the various mapping levels. Also, paired sets of small arrows are used to show connection between separate bodies of tracer observed at the same level.

level of detail removed in generating Figure 7 (note all of the original hand drawn maps were digitized and are given by *Nicholl and Glass* [2002]). The tracer domains are stacked vertically in Figure 8 to further illustrate spatial variability within the relatively shallow depth (~5 m) of this excavation. The flow field clearly spread beyond the region of detailed mapping to produce an irregular structure that occupied ~35 m^3 of the excavated rock mass and obviously extended below the ~5 m depth of excavation. In addition, complication of the dye structure within the fracture network varied from pervasive stain near the infiltration surface, to more fragmented and intricate structures at depth where the flow field appears to have bypassed a significant fraction of the network. Observed penetration of dye into the matrix was negligible across the entire excavated region, confirming that flow was constrained to the fracture network. In this section, we first describe the fracture network geometry and dye tracer structure. We then present ERT data, followed by estimates for the mean and effective hydraulic aperture of fractures adjacent to the pond, and the volume of rock that may have been interrogated by this test. Finally, we conclude by discussing the implications of our results with respect to the design of potential future field experiments.

3.1. Fracture Network Geometry

[14] The fracture network exhibited strong connectivity in both the horizontal and vertical planes. While the excavation method did not allow us to follow individual fractures in the vertical direction, it was clear that a number of extensive near-vertical fractures passed through the mapped prism. In particular, all pavement maps (Figure 7) show an extensive fracture (marked on the figures with a black square) beginning slightly north of the SW corner and trending toward the NE corner. In some maps, this fracture appears to be broken into segments; an observation that we believe to be a mapping artifact rising from the roughness of the excavation surface. In the excavation walls, steeply dipping fractures were observed to extend from land surface down through the bottom of the excavation, a distance of greater than 6 m. We also observed truncated subhorizontal features with trace lengths on the order of 2 m. Nearby, *Throckmorton and Verbeek* [1995] reported steeply dipping fractures with heights of up to 12 m, and truncated lengths of 6–10 m; they also reported subhorizontal fractures with lengths of 5+ m. Such extensive and closely spaced fractures in orthogonal sets will produce a very well connected network. Multiple episodes of fracturing [*Throckmorton and Verbeek*, 1995] from a variety of mechanisms (cooling, tectonic, erosional unloading) will also have enhanced connectivity, as later fractures are expected to terminate into the earlier ones.

[15] Of the 741 fractures that we measured, most (~60%) extended outside of the 2.4 × 2.4 m mapped area; for the remaining 40%, the probability of occurrence (p) for a specific trace length (l) fit the exponential model ($p = e^{-cl}$) suggested by *Call et al.* [1976], with c = 1.7. On 572 of the measured fractures, at least one of the fracture surfaces was exposed, and we were able to measure dip. Small aperture, near-vertical fractures often broke flush with the pavement surface, preventing us from measuring dip. Fracture orientation data (Figure 9) show two strong near-vertical sets: one

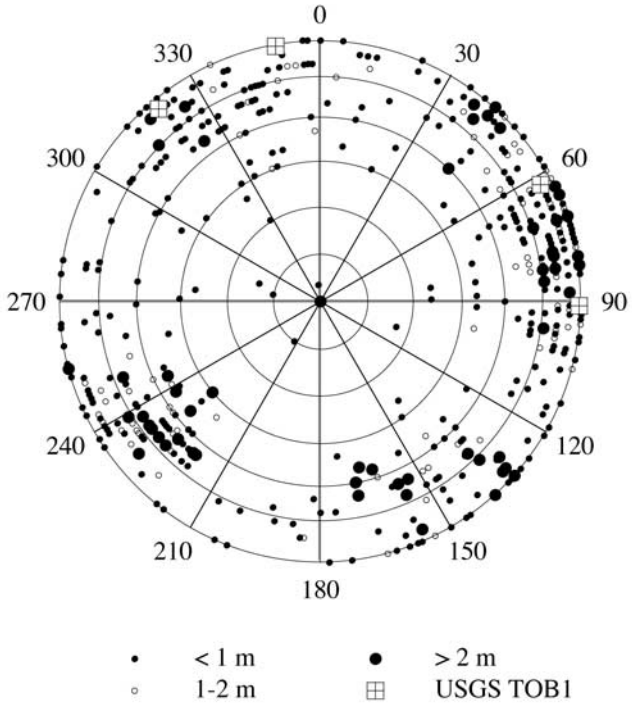

Figure 9. Fracture orientations. Dip was measured for 77% of the mapped fractures. Poles of the measured planes are plotted on a polar equal-area projection. Data are divided into three groups on the basis of measured trace length (0–1 m, 1–2 m, and >2 m). Data show at least two sets of steeply dipping, extensive (trace length >2 m) fractures. Measured orientation of the smaller fractures shows more scatter than that for the extensive features. Our data are consistent with USGS measurements at an adjacent site (USGS TOB1, marked as pit #1 on Figure 1) reported by *Throckmorton and Verbeek* [1995].

trending to the NW/SE, and the other to the SW/NE. The extensive near-vertical fractures (>2 m trace length) maintain consistent orientation with depth, and exhibit less variability than the smaller features. *Throckmorton and Verbeek* [1995] measured two test pits (~4–5 m deep) and pavement areas immediately (several meters) south and west of our experiment (Figure 1). In the location closest to our experiment (pit #1), they reported two sets of steeply dipping cooling joints, and two younger sets of steeply dipping tectonic joints; orientation of those sets are consistent with our measurements (Figure 9).

[16] Horizontal pavements preferentially sample steeply dipping fractures, and under sample those with a shallow dip (subhorizontal). Furthermore, the excavation method tended to damage and fragment the surface of subhorizontal features. As a result, our measured data (Figure 9) are overwhelming weighted toward steeply dipping fractures. However, we did note subhorizontal fractures at most excavation levels, particularly at shallower depths, and numerous examples were observed in the excavation walls. These undulating fractures appeared to dip slightly in the general direction of the topography (north and east), which is consistent with data from the adjacent pit [*Throckmorton and Verbeek*, 1995]. They reported two sets of subhorizontal fractures, one dipping ~10° to the SE, and the other ~5° to the NE; the first set was attributed to cooling, and the second to erosional unloading. They also report fracture spacings for subhorizontal fracture on the order of 0.3–1 m, with localized zones spaced on the order of 5 cm.

3.2. Dye Tracer Structure

[17] We first consider the gross outer extent of the dyed structure. At the infiltration surface, dye was only observed on fractures within the surface pond (Figure 7, level 0). However, with increasing depth, estimated extent of the flow field first expands and then contracts (see Figure 10). Directly below the infiltration surface (Figure 7, level 1), dye was observed both inside and outside (to the north and east) of the mapped area. Over the next intervals, expansion and contraction of the stained area occurred in all directions except SW, where a persistent near-vertical fracture appeared to form a barrier that separated stained and unstained regions. At depths of 1–4 m (levels 3–8), the dyed structure appeared to expand as several disjoint appendages. The surface of a vertical fracture exposed in the south wall of the excavation was partially (0.2–0.5 m^2) stained. While this fracture did not pass through the mapped region, it clearly connected with two near-vertical fractures that did. A persistent SW–NE trending fracture that dissected the mapped area (described in section 3.1) clearly showed dye stain NE of the mapped area. In that direction, small dye stains were observed 2–3 m NE of our mapped area in near-vertical fractures exposed along the face of a 1 m buffer zone surrounding the LBT block. We also noted a subhorizontal fracture exposed in the south wall of the excavation (level 7) that showed stain over a ~1.5 m long portion of its length. At level 8, pavement extending to the N and NW of the mapped area showed heavy stain, as did rubbelized rock excavated 3–4 m to the north. At level 10, dye stain was noted in the south wall of the excavation ~3 m east of our mapped area. By the bottom of the excavation (level 11), all but one of these appendages appeared to have

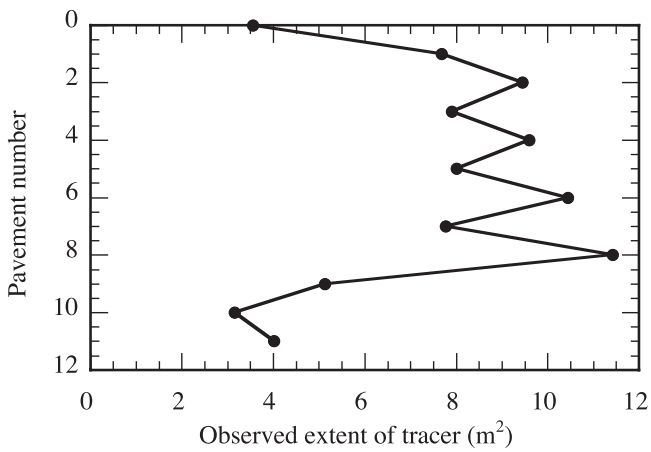

Figure 10. Estimated extent of tracer at each level of the excavation. Areas taken from Figure 7 are plotted as a function of pavement number; on average, pavements were separated vertically by ~0.5 m. Estimated extent of the flow field is seen to increase rapidly immediately below the infiltration pond, oscillate near the larger value, and then, near the bottom of the excavation, area contracts to approximately that of the original pond.

died out, and in the final three levels (9–11), the stained region contracted to approximately the same area as the original pond.

[18] Focusing next on the pavement maps alone, we obtain a representative and detailed record of tracer distribution within the ~30 m^3 prism directly below the infiltration surface. Immediately (<1 m) below the infiltration pond, all fracture surfaces except those in the extreme SW corner of the mapped region were completely stained, including the few exposures of subhorizontal features that were undamaged by excavation. At greater depth (2–3 m and below), distribution of tracer within the mapped region became complicated and fragmented, as exemplified in Figure 5 (level 8). Many fractures were not stained, and others only partially so, often despite obvious physical connection to stained portions of the network. On some long, near-vertical fractures, stain was restricted to portions of the fracture trace, yielding alternating bands of stained and unstained regions.

[19] The observed changes in phase complication with depth (pervasive near the pond to fragmented and intricate with significant network bypass at depth) are expected based on studies in single fractures. There, it has been shown that accessibility and competition between viscous, gravitational, and capillary forces influences the complexity of a developing phase structure [*Glass et al.*, 2001]. When viscous forces and accessibility are high, such as occur near the surface pond, phase structure should be simple and fractures fully saturated. With depth, pressure will transition from positive (saturated) to negative (unsaturated) as the relative importance of capillary forces increases. The transition into unsaturated conditions causes capillary heterogeneity, gravity, and the role of fracture intersections to show themselves by fragmenting the phase structure, and creating complication within both the network and individual fractures [*Glass et al.*, 1995, 1996].

[20] Slow displacement of a nonwetting fluid by a wetting fluid along the plane of a horizontal fracture can bypass large portions of the fracture plane to produce phase structures exhibiting a level of complexity similar to that seen in Figure 6b [*Glass et al.*, 1998]. As compared to a fully saturated fracture, the wetted structure implied from Figure 6b would produce a greatly reduced permeability [*Nicholl et al.*, 2000], restrict water phase connection between adjacent matrix blocks, and afford smaller contact area for imbibition into the adjacent matrix [*Glass et al.*, 1995, 1996]. In nonhorizontal fractures, a number of studies have considered the formation of gravity-driven fingers where flux drops below the product of saturated conductivity of the fracture and the gravitational gradient [e.g., *Nicholl et al.*, 1992, 1993a, 1993b, 1994; *Glass*, 1993; *Glass and Nicholl*, 1996; *Su et al.*, 1999]. This condition is expected to occur within the fragmented field away from the ponded source, and produce structures elongated in the direction of gravity. Gravity-driven fingers advance at velocities considerably higher than the average flux rate, wet a small fraction of the aperture field, and travel a greater distance than a uniform front of equivalent volume. While we found numerous instances where the pavement was stained along short (2–10 cm) lengths of a fracture (see Figure 5), and Figure 6c is more likely a gravity-driven finger than an image of the rare blue rock scorpion, we can not conclusively differentiate these observations from capillary driven flow through smaller aperture regions. A similar dilemma was faced by *O'Hara et al.* [2000] in interpreting DNAPL distribution during disassembly of an intermediate scale (0.5 m diameter) fractured clay core.

[21] Finally, we emphasize the wide variety of tracer configurations found at fracture intersections (e.g., Figure 5). In some places, the surfaces of both fractures were fully stained (i.e., stain was continuous along each fracture for a significant distance away from the intersection). In other locations, one fracture was fully stained around the intersection, while the other showed no evidence of tracer. We also noted instances where one or both of the intersecting fractures were only stained in the immediate vicinity (2–15 cm) of the intersection. Occasionally, small spots of tracer were observed on subhorizontal fractures; on closer inspection, it was discovered that these locations corresponded to intersections between vertical hairline fractures. The excavation method did not expose the surfaces of many vertical fractures; however, some showed dark tracer stains along the lower edge that faded in color upward before disappearing, suggesting the fracture below to have formed a capillary barrier that possibly concentrated flow. In such a scenario, a downward moving finger would be at insufficient pressure to cross the open aperture of an intersecting fracture. Liquid would pool above the barrier, migrating laterally along the intersection and upward. With further flow, rising pool height would increase pressure at the barrier until it breached at one (low flow conditions) or more (high flow conditions) locations; a finger would form below each breach in the capillary barrier and continue downward. Such pooling would also allow flow from multiple fingers to coalesce above the intersection, thus causing the confluence of flow [*Glass et al.*, 1995, 1996].

3.3. ERT

[22] Voltage and current measurements from the electrode array were processed to produce tomographic images of electrical resistivity (data collection and processing methods are discussed by *Ramirez and Daily* [2001]). Briefly, the algorithm uses a combination of forward and inverse numerical modeling procedures to find a smooth resistivity field that fits the data to a prescribed tolerance [see *LaBrecque et al.*, 1996]. Although the solution domain is much larger (28 m wide and 35 m tall), we limit our interpretation to the region inside the ERT electrode arrays where data is best constrained. In this region, a 0.15 × 0.15 m grid resolution leads to two-dimensional images of electrical resistivity over 1.5 m wide × 3 m high vertical planes along the principal diagonals of the ERT array (see string locations on Figure 2). Changes in resistivity resulting from the addition of water (decreased resistivity) and subsequent drainage (increased resistivity) were highlighted by normalizing images to data collected the day prior to infiltration. It is important to recognize that the shapes of the resistivity anomalies calculated by the ERT algorithm may be distorted for the following reasons. (1) The inversion algorithm finds a smooth resistivity field with anomalies that are larger in area than the target fractures. (2) The amount of time required to complete an ERT survey was large compared to the timescale for liquid phase development within the fracture network; in other words, the

"shutter speed" on our "camera" was slow, thereby resulting in some "smearing" of the resistivity anomalies. (3) Data were collected and inverted over two-dimensional planes, while the fracture network and the flow of electricity was fully three-dimensional. (4) The flow field clearly passed outside of our instrumented prism; moisture outside of the ERT array is expected to have a reduced but difficult to quantify influence on resistivity measurements.

[23] Normalized resistivity images within the plane between strings 1 and 3 were constructed for time periods of 2–24, 24–44, 77–99, and 1320–1342 min after infiltration was started (Figure 11a). By 2–24 min, sharp decreases in resistivity are seen to extend from the surface pond through the base of the 3 m imaging depth. At any given depth, numerous (10–15) near-vertical fractures cross the 1–3 imaging plane (see Figure 7, levels 0–7); localization of decreased resistivity in the ERT image suggests significant preferential flow within the pervasive fracture network. At 24–44 min, we see zones where resistivity has decreased, apparently from continued wetting of the fracture network; however, we also see zones where resistivity has increased. Noting that the surface pond broke into a series of puddles between 36 and 45 min, zones of increased resistance could be associated with rapid drainage of the network. In both images taken during infiltration (2–24 and 24–44), the surface pond exerts a strong influence on measured resistivity (i.e., bright red zone at the top of both images). At 77–99 min, resistivity has returned to near pretest levels both at the top of the image (directly beneath the pond) and at the bottom of the image; meanwhile, the zone in the middle of the plane shows a decrease in resistivity that suggests a further lateral wetting of the region, or maybe even the formation of a new connected pathway that sweeps down from the top left to near the center of the image. However, this zone of decreased resistivity could also simply be an ERT imaging artifact; as the electrical connectivity changes within the fracture network on depletion of the surface pond, the now drained channel originally on the left in the two earlier images could be shifted by the inversion algorithm toward the center. Finally, an image taken on the following day (1320–1337 min) shows only a slight additional increase in resistivity (water drainage).

[24] Additional perspective on the drainage process is provided by images across the plane between strings 2 and 4 (Figure 11b) taken after the surface pond was depleted. Between 52–74 min and 114–136 min we see what appears to be drainage from the top quarter of the image (as well as from outside the plane) into parts below through the formation of some new pathways. Over the subsequent day, drainage continued with a return to a near uniform background condition at 1370–1392 min. The 2–4 plane indicates more horizontal connection than the 1–3 plane, with some behavior suggestive of horizontal fractures acting as capillary barriers.

[25] Across all images, significant features can be seen down to scales on the order of the typical separation distance between adjacent electrodes (30 cm). We know from our mapping that pervasive flow near the surface began to fragment at a depth of 2–3 m. This generally supports the ERT data, where zones in both the 1–3 and 2–4 planes that did not experience a resistance lowering only appear in the bottom half of the plane. However, for the reasons discussed above, ERT images are subject to various distorting influences; hence, we cannot ascertain how well these interpretations reflect the actual evolution of phase structure. Certainly, at a minimum, ERT results demonstrate rapid vertical penetration of the fracture network, followed by rapid drainage to a moisture content at some value above the initial state. At a maximum, the data suggest significant preferential flow within the network, the action of horizontal fractures as capillary barriers, formation of new pathways during drainage, and the lateral shifting of existing pathways during drainage. Clearly, further research that considers the application of ERT to define phase structure evolution within fractured rock formations is required before unambiguous interpretations can be made.

3.4. Estimation of Mean and Effective Hydraulic Apertures

[26] Although time constraints prohibited measuring fracture apertures on the excavated pavements, we can estimate mean aperture $\langle b \rangle$ near the infiltration surface by calculating an effective hydraulic aperture b_h. Assuming saturated vertical flow under unit gradient through fractures of total length, L, Darcy's Law for flow, Q, across the infiltration surface can be rearranged to yield

$$b_h^3 = \frac{12Q\upsilon}{gL},$$

where v is kinematic viscosity of the liquid, and g is the acceleration due to gravity. The measured length of fractures in the infiltration pond totaled ~33 m; given Q of 0.26 L/s for times >10 min, and assuming that liquid viscosity was that of pure water at 25°C, leads to an estimate of 0.02 cm for b_h. Noting that b_h varies with the cube root of these quantities, uncertainty in flow rate, liquid viscosity, and fracture length have only a small effect on our estimate for b_h. However, there is a fair degree of uncertainty associated with the estimation of $\langle b \rangle$ by b_h. In discrete fractures, three-dimensional flow acts to reduce the permeability of a rough-walled fracture with respect to two-dimensional flow between parallel plates; therefore, one normally expects b_h to be somewhat smaller than $\langle b \rangle$ [e.g., *Brown et al.*, 1995]. However, well-connected large aperture regions that form high permeability conduits through the system will tend to compensate for this underestimate (i.e., increase b_h relative to $\langle b \rangle$). Features of fracture networks with the potential to produce connected large aperture regions include fracture intersections, shatter zones, and individual open fractures.

3.5. Possible Range of Rock Volume Interrogated by Infiltration

[27] Approximately 35 m^3 of excavated rock mass was contacted by the flow field; however, the infiltration pulse clearly penetrated beneath the ~5 m depth of excavation. Additionally, within the 35 m^3 contacted, a large fraction of the network was bypassed, and ERT data demonstrated subsequent drainage. To estimate the possible range of rock volume interrogated by our short ponding event, we consider a series of approximations based on measurements or inferences. First, we estimate the volume of water required to fully saturate the fracture network (i.e., fracture porosity).

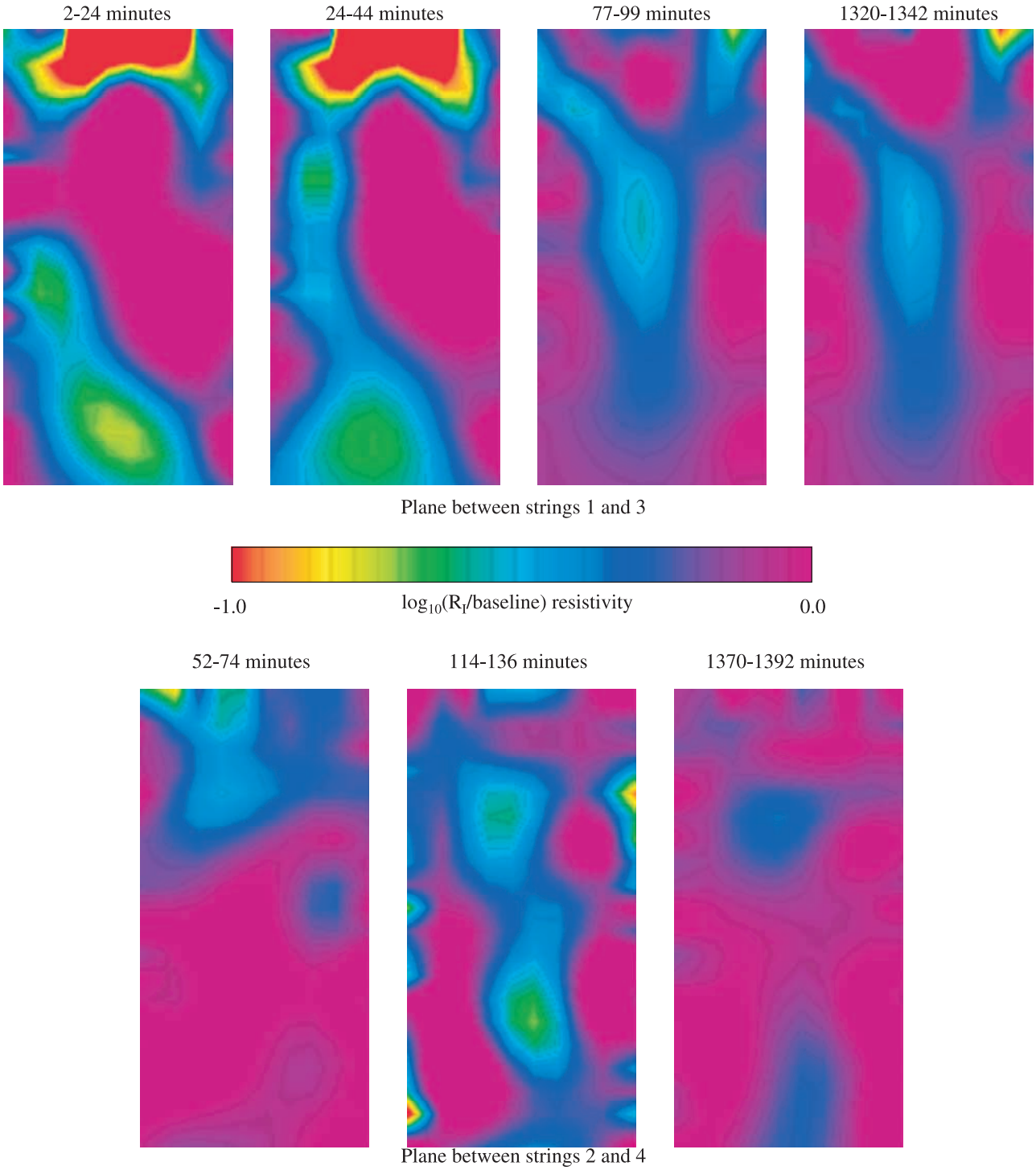

Figure 11. ERT Images. All resistivity images were calculated from data collected over a 22 min period, and represent a 1.5 m wide by 3.0 m deep plane between the electrode strings noted in Figures 2 and 7. In order to highlight changes resulting from the addition of water, images of resistivity following infiltration (R_I) were normalized to baseline images taken the day previous to the infiltration test; results are presented as log10 (R_I/baseline) as depicted in the color bar. (a) Images constructed between strings 1 (left side of the resistivity image) and 3 (right side) at times during early infiltration (2–24 min), late infiltration with the onset of drainage (24–44 min), early drainage (77–99 min), and late drainage (1320–1337 min). (b) Images constructed between strings 2 (left side) and 4 (right side) at times during early drainage (52–74 and 114–136 min) and late drainage (1370–1392 min).

Measurement of the pavement maps at levels 1–6, 8, and 11 yield a volumetric density for the steeply dipping fractures of ~10 m^2/m^3. The remaining maps were ignored because the level of detail was adversely affected by the infiltration basin (level 0) and construction activity (levels 7, 9, and 10). Measurements reported by *Throckmorton and Verbeek* [1995] and observation of the excavation walls suggest a volumetric density for the subhorizontal fractures on the order of ~2 m^2/m^3, giving a total fracture density of ~12 m^2/m^3. Assuming that b_h (see section 3.4) provides a first-order estimate for the mean aperture leads to a fracture porosity of $\sim 2.4 \times 10^{-3}$, or 2.4 L/m^3.

[28] Next, we acknowledge that some matrix imbibition will have occurred during the period of our test and thus increase the 'storage capacity' of the rock mass. To estimate an imbibition volume, we took several large samples from the excavated rock mass, cut them into blocks (~1500–7500 cm^3), dried them, and then submerged them in water. We note that microfractures present in all of these samples contributed to our imbibition measurements. For all samples, imbibition in time fit a power law; for the length of our ponding event (46 min) imbibition by the four samples averaged ~0.033 L per m^2 of surface area (imbibition by individual samples ranged between 0.025 and 0.041 L/m^2). Combining this result with fracture surface area (twice the volumetric density) leads to an estimate for matrix imbibition of ~0.8 L/m^3 over a 46 min period. The sum of aperture volume and matrix imbibition is 3.2 L/m^3, suggesting that our infiltration event (790 L) would have fully saturated the fracture network and satisfied matrix imbibition in a volume of ~250 m^3, 7 times greater than the ~35 m^3 that we observed in the excavation.

[29] Beyond this simple estimate, additional inferences suggest the possibility of a much greater interrogated volume. ERT data show that the liquid slug redistributed after the pond was exhausted. Water draining from near-surface fractures will continue to supply the advancing infiltration front and allow further penetration of the network. Values of fracture saturation following drainage could be in the range of 0.2–0.5, causing our estimate to increase by a factor of 2 to 5. We also found that except near the infiltration surface where viscous forces led to pervasive flow, phase structure within the excavation was fragmented and covered only a fraction of the network. If we conservatively estimate the fraction of the network contacted at 0.1–0.5, and combine this estimate with drainage saturations between 0.2 and 0.5, then the volume of rock contacted by our flow field would increase over the saturated estimate by a factor ranging from 4 to 50.

[30] All of these estimates suggest that our excavation revealed only from ~15% (fully saturated volume) to far less than 1% (including redistribution and structural fragmentation) of the total volume of rock that our experiment could have traversed. We emphasize that these estimations are all premised on the assumption that properties of the rock mass and fracture network (matrix, fracture density, connectivity) continue unchanged with depth. If this is the case and if the gross structure seen in Figure 8 is maintained with depth, water from our slug would have initially penetrated to a depth of at least ~35 m, and then redistributed to an eventual depth of at least 140 m, a significant depth considering the short duration of the ponded source. However, at least two processes may curtail such an extreme penetration. First, the continued fragmentation of the liquid body could increase the importance of capillary heterogeneity within the formation and cause greater pathway excursions in the horizontal. Second, after ponding, velocities within the field will slow and thus the timescale for matrix imbibition at a given location will increase beyond the 46 min representative of the near surface zone. Clearly, even if we ignore the probability of significant changes in rock mass character with depth, predicting the penetration depth of a surface infiltration event is, at present, highly speculative, and underscores our vast ignorance of phase structure development in fractured rock formations.

3.6. Implications With Respect to Future Field Experiments

[31] Our ponded infiltration test produced a final phase structure that varied from pervasive to complex. Unfortunately, a single field test such as this cannot evaluate the competing influences of capillary, gravity, and viscous forces within the fracture network. Could an experimental design be formulated that would yield this information? Let us envision a design where multiple experiments within a single, well-characterized natural fracture network could be conducted. Imagine a series of infiltration experiments where the network is returned to the original initial conditions between trials. A different flow rate and tracer could be used for each test; not only would each tracer have to be easily discernable, it would also have to strongly adsorb to the fracture surfaces in order to prevent remobilization during subsequent experiments. ERT, appropriately evaluated for accuracy and resolution, could be employed to follow the temporal dynamics of the phase structure evolution, while point sensors could capture pressure and saturation observations with high temporal resolution. At the conclusion of such an experiment, one would carefully disassemble the rock mass to map the geometry of the fracture network (including the aperture field variation) and distribution of the various tracers in three dimensions. While at first glance such an experiment would seem to be possible, there are significant issues which must be considered.

[32] In our experiment, ERT was able to detect changes in resistivity resulting from infiltration, and clearly showed rapid invasion of the fracture network, followed by rapid drainage. While this and subsequent work on the LBT [*Ramirez and Daily*, 2001] demonstrates the utility of ERT in our host rock, a number of open questions remain regarding the ability of geophysical techniques to obtain data at sufficient accuracy or resolution (spatial, temporal) to delineate phase structure and dynamics within discrete fracture networks. In order to discriminate between various competing flow processes we must be able to: resolve individual, partially saturated fractures oriented at various angles to the measurement direction; identify which of many fractures actually fills with water or drains; and, delineate phase structure within those fractures. Even with precise knowledge of network geometry, it is unlikely that techniques which integrate over volumes on the order of thousands of cm^3 or greater (such as ERT) will be able to provide information at the required level of detail. The

problem is further exacerbated if transient pulses move through vertical fractures much faster than the data collection time, as occurred in our experiment. Planning the domain to be monitored before the experiment is another issue. Here, we considered gravity-driven infiltration in a system characterized by pervasive and extensive vertical fractures. Based on those characteristics, we designed our ERT array to extend directly below the infiltration pond. Yet the flow field exhibited significant and highly variable behavior in the lateral plane that would have been difficult to predict at the design stage, and thus we obtained only limited coverage.

[33] In addition, we note that instrumenting a field test in fractured rock with either geophysical arrays or devices that yield point measurements (e.g., saturation, pressure) raises significant issues regarding system perturbation. Drilling adds microfractures to the system, and may form capillary bridges across open fractures by creating shatter zones or forcing cuttings into the aperture. Grouted boreholes may act as conduits, barriers, liquid sinks, or bridges, while liquid in the grout (or drilling fluid) may be drawn into the adjacent matrix or small aperture fractures; open boreholes may provide conduits for liquid and vapor transport. In our test, four vertical holes were dry drilled and instrumented with ERT electrode strings that were grouted in place. While we did not see any severe disturbances due to these procedures in our excavation, we cannot discount the possibility that they did indeed influence the phase structure development.

[34] Finally, we note that recreating the original initial conditions between trials may be a physical impossibility. Drying out the network would be problematic, particularly if water imbibes into the rock matrix or fracture filling. There is also the potential for alteration of the fracture network itself by the experiment. Use of adsorptive tracers would likely affect surface chemistry, as would any biologic activity resulting from introduction of water into an initially dry system. Also, the use of disequilibrium liquids could affect system geometry, particularly small aperture regions, by eroding fracture coatings and mobilizing fine material. Regardless, return to the original initial condition must be verified, which in itself may be truly impossible.

4. Concluding Remarks

[35] The phase structure observed beneath the surface pond in our field experiment was generally consistent with expectations based on laboratory experiments in single fractures. Although details of the phase structure are determined by site specific and experimental (initial/boundary) conditions, we expect that the salient behavior of fragmentation and structural complexity are fundamental characteristics that will appear when infiltration is critically influenced by the fracture network. Near the pond, high invasion rates and liquid pressures combined with a complete connection to the source to produce a fully stained network. The phase structure immediately expanded beneath the pond; with depth, the structure became fragmented and complicated. Variability in the large-scale lateral extent of the flow field is expected from the inherent variability of individual fractures and their connectivity within the network. Additionally, fragmentation and complication are expected away from the pond as viscous forces decrease relative to capillary and gravity forces. We saw evidence of preferential flow, fingers, irregular wetting patterns, and varied behavior at fracture intersections; all of which have implications with respect to flow/transport in unsaturated fractured rock, and the design of future experiments. Finally, ERT data show that infiltration was followed by drainage once the pond was depleted, both processes occurring rapidly.

[36] While our single experiment cannot be used to rigorously test hypothesized system behavior, it has given us an enhanced appreciation of both the complexity of unsaturated flow in a fracture network, and the potential for a seemingly innocuous ponded infiltration event to result in unexpectedly deep penetration. Under natural conditions within arid fractured rock catchments, we expect that the topographic confluence of surface water at the upland beginnings and subsequent flow down washes will commonly cause surface ponding at durations similar to, or longer than what we imposed in our test. At locations where alluvium is either nonexistent (upland beginnings) or has been washed away, the fracture network will be open for water to enter directly, such as was explored in our experiment. Indeed, geochemical data from fractured tuffs at both Apache Leap, Arizona [*Davidson et al.*, 1998], and only a few miles from our experiment at Yucca Mountain, Nevada [*Fabryka-Martin et al.*, 1996; *Yang et al.*, 1996], have demonstrated that natural conditions can lead to the deep penetration of unsaturated fractured rock by meteoric water.

[37] We recognize a number of limitations in our measurements that affected our ability to characterize the fracture network, phase structure of the flow field, and temporal evolution of the system. However, despite these limitations, our data set provides a glimpse at phase structure in an unsaturated natural fracture network. A simple modeling study based on these data has been reported by *Eaton et al.* [1996a, 1996b] where both dual-permeability and equivalent-continuum approaches were applied. As one might expect, the two approaches resulted in strikingly different saturation distributions. And of course, neither displayed the rich variety of behavior observed in the field. Further modeling with increased complication, i.e., discrete fracture approaches, would yield a next iteration, and the incorporation of more heterogeneity could yield a closer correspondence to experiment. However, such a study must be carefully designed so that understanding is increased beyond simple 'heterogeneity calibration;' we must remember that all such simulation is constrained by assumptions in the underlying conceptual model and limitations resulting from the numerical implementation.

[38] Our observations raise issues concerning the design of field experiments that will improve our fundamental understanding of flow processes in unsaturated fractured rock. The variable and complicated nature of our phase structure implies a need for such detailed and extensive spatial coverage that installation of point-sensing devices would necessarily disrupt the natural system. Conversely, geophysical techniques that give spatial or temporal averages may not detect, or may misrepresent a complicated and evolving flow structure. Because of these limitations, field experiments may not allow us to conclusively discriminate between the influences of material heterogeneity (e.g., net-

work geometry) and those of unsaturated flow physics (e.g., competition between viscous, gravity, and capillary forces) in determining observed phase structure. Instead, mesoscale (one to several meters) laboratory experiments are required to appropriately consider the growth and dynamics of phase structure within fracture and fracture–matrix networks. There, one can systematically vary parameters to explore the relative importance of material properties and fundamental flow processes in generating structure, as well as additional influences due to coupled geomechanical, geochemical, and biological processes.

[39] **Acknowledgments.** Our field experiment was designed and conducted in the spring of 1994, with support from the U.S. Department of Energy, Office of Civilian Radioactive Waste Management, Yucca Mountain Site Characterization Project Office, under contract DE-AC04-94AL85000 (Sandia National Laboratories (SNL)) and W-7405-ENG-48 (Lawrence Livermore National Laboratory (LLNL)). Original data are contained in Sandia National Laboratories Yucca Mountain Project controlled scientific notebooks MOL.19961029.0104 and MOL.19961029.0110, and Lawrence Livermore National Laboratories Yucca Mountain controlled scientific notebook LBT-03, 3/4/94, pp. 5–26. R.J.G and M.J.N. gratefully acknowledge additional support from the U.S. Department of Energy, Basic Energy Sciences Geoscience Research Program under contract numbers DE-AC04-94AL85000 (Sandia National Laboratories) and DE-FG03-01ER15122 (University of Idaho) that allowed the analysis, interpretation, composition, and publication of this paper. Mapping assistance was provided by D. Engstrom and S. McKenna of SNL. C. Rautman (SNL) provided invaluable assistance regarding the general geology of Yucca Mountain. This work could not have occurred without the assistance of W. Lin and M. Owens of LLNL. Finally, we would like to thank N. Weisbrod and an anonymous reviewer for their thorough and constructive comments on this manuscript.

References

Bedinger, M. S., K. A. Sargent, and W. H. Langer, Studies of geology and hydrology in the basin and range province, southwestern United States, for isolation of high-level radioactive waste—Evaluation of the regions, *U.S. Geol. Surv. Prof. Pap., 1370-H*, 61 pp., 1990.

Bekri, S., J. F. Thovert, and P. M. Adler, Dissolution and deposition in fractures, *Eng. Geol.*, *48*(3–4), 283–308, 1997.

Brown, D. A., D. C. Kamineni, J. A. Sawicki, and T. J. Beveridge, Minerals associated with biofilms occurring on exposed rock in a granitic underground research laboratory, *Appl. Environ. Microbiol.*, *60*, 3182–3191, 1994.

Brown, S. R., H. W. Stockman, and S. J. Reeves, Applicability of the Reynolds equation for modeling fluid flow between rough surfaces, *Geophys. Res. Lett.*, *22*, 2537–2540, 1995.

Bussod, G. Y., H. J. Turin, and B. A. Robinson, Unsaturated zone tracer testing at Busted Butte, Nevada: Phase 1 results and model predictions, *Geol. Soc. Am. Abstr. Programs*, *31*(7), A-491, 1999.

Call, R. D., J. P. Savely, and D. E. Nicholas, Estimation of joint set characteristics from surface mapping data, paper presented at 17th US Symposium on Rock Mechanics, Am. Inst. of Min., Metal., and Pet. Eng., Snowbird, Utah, 25–27 Aug. 1976.

Dahan, O., R. Nativ, M. Adar, B. Berkowitz, and Z. Ronen, Field observation of flow in a fracture intersecting unsaturated chalk, *Water Resour. Res.*, *35*(11), 3315–3326, 1999.

Davidson, G. R., R. L. Bassett, E. L. Hardin, and D. L. Thompson, Geochemical evidence of preferential flow of water through fractures in unsaturated tuff, Apache Leap, *Appl. Geochem.*, *13*, 185–195, 1998.

Drier, R. B., D. K. Solomon, and C. M. Beaudoin, Fracture characterization in the unsaturated zone of a shallow land burial facility, in *Flow and Transport Through Unsaturated Fractured Rock*, *Geophys. Monogr. Ser.*, vol. 42, edited by D. D. Evans and T. J. Nicholson, pp. 51–59, AGU, Washington, D. C., 1987.

Eaton, R. R., C. K. Ho, R. J. Glass, M. J. Nicholl, and B. W. Arnold, Modeling of flow through fractured tuff at Fran Ridge, paper presented at 7th International Conference of High Level Radioactive Waste Management, Am. Nucl. Soc., Las Vegas, Nev., 29 April to 3 May 1996a.

Eaton, R. R., C. K. Ho, R. J. Glass, M. J. Nicholl, and B. W. Arnold, Three-dimensional modeling of flow through fractured tuff at Fran Ridge, *SAND95-1896*, 60 pp., Sandia Natl. Lab., Albuquerque, N. M., 1996b.

Fabryka-Martin, J. T., P. R. Dixon, S. S. Levy, B. Liu, D. L. Brenner, L. E. Wolfsberg, H. J. Turin, and P. Sharma, Implications of environmental isotopes for flow and transport in the unsaturated zone at Yucca Mountain, Nevada, *Geol. Soc. Am. Abstr. Programs*, *28*(7), A-416, 1996.

Faybishenko, B., C. Doughty, S. Steiger, J. Long, T. Wood, J. Jacobsen, J. Lore, and P. Zawislanski, Conceptual model of the geometry and physics of water flow in a fractured basalt vadose zone, *Water Resour. Res.*, *36*(12), 3499–3520, 2000.

Gimmi, T., M. Schneebeli, H. Fluhler, H. Wydler, and T. Baer, Field-scale transport in unsaturated crystalline rock, *Water Resour. Res.*, *33*(4), 589–598, 1997.

Glass, R. J., Modeling gravity driven fingering in rough-walled fractures using modified percolation theory, paper presented at 4th International Conference on High Level Radioactive Waste Management, Am. Nucl. Soc., Las Vegas, Nev., 26–30 April 1993.

Glass, R. J., and M. J. Nicholl, Quantitative visualization of entrapped phase dissolution within a horizontal flowing fracture, *Geophys. Res. Lett.*, *22*(11), 1413–1416, 1995a.

Glass, R. J., and M. J. Nicholl, Near drift two-phase flow processes within regionally saturated fractured rock, paper presented at the Sixth Annual International Conference on High Level Radioactive Waste Management, Am. Nucl. Soc., Las Vegas, Nev., 1–5 May 1995b.

Glass, R. J., and M. J. Nicholl, Physics of gravity-driven fingering of immiscible fluids within porous media: An overview of current understanding and selected complicating factors, *Geoderma*, *70*, 133–163, 1996.

Glass, R. J., M. J. Nicholl, and V. C. Tidwell, Challenging models for flow in unsaturated, fractured rock through exploration of small scale flow processes, *Geophys. Res. Lett.*, *22*(11), 1457–1460, 1995.

Glass, R. J., M. J. Nicholl, and V. C. Tidwell, Challenging and improving conceptual models for isothermal flow in unsaturated, fractured rock through exploration of small scale processes, *SAND95-1824*, 61 pp., Sandia Natl. Lab., Albuquerque, N. M., 1996.

Glass, R. J., M. J. Nicholl, and L. Yarrington, A modified invasion percolation model for low capillary number immiscible displacements in horizontal rough walled fractures: Influence of local in-plane curvature, *Water Resour. Res.*, *34*(12), 3215–3234, 1998.

Glass, R. J., H. Rajaram, M. J. Nicholl, and R. L. Detwiler, The interaction of two fluid phases in fractured media, *Colloid Interface Sci.*, *6*, 223–235, 2001.

Hanna, R. B., and H. Rajaram, Influence of aperture variability on dissolutional growth of fissures in karst formations, *Water Resour. Res.*, *34*(11), 2843–2853, 1998.

Kilbury, R. K., T. C. Rasmussen, D. D. Evans, and A. W. Warrick, Water and air intake of surface-exposed rock fractures in situ, *Water Resour. Res.*, *22*(10), 1431–1443, 1986.

LaBrecque, D. J., M. Miletto, W. Daily, A. Ramirez, and E. Owen, The effects of noise on Occam's inversion of resistivity tomography data, *Geophysics*, *61*, 538–548, 1996.

Lin, W., D. G. Wilder, J. A. Blink, S. C. Blair, T. A. Buscheck, D. A. Chesnut, W. E. Glassley, K. Lee, and J. J. Roberts, The testing of thermal–mechanical–hydrological–chemical processes using a large block, paper presented at the Fifth Annual International Conference on High Level Radioactive Waste Management, Am. Nucl. Soc., Las Vegas, Nev., 22–26 May 1994.

Lin, W., S. Blair, D. Wilder, W. Carlson, J. Wagoner, L. DeLoach, G. Danko, A. Ramirez, and K. Lee, Large block test final report, *UCRL-ID-132246*, Lawrence Livermore Natl. Lab., Livermore, Calif., 2001.

Liu, H. H., C. Doughty, and G. S. Bodvarsson, An active fracture model for unsaturated flow and transport in fractured rocks, *Water Resour. Res.*, *34*(10), 2633–2646, 1998.

National Research Council, *Rock Fractures and Fluid Flow*: *Contemporary Understanding and Application*, pp. 127–132, edited by Comm. on Fracture Characterization and Fluid Flow, Natl. Acad. Press, Washington, D. C., 1996.

Nicholl, M. J., and R. J. Glass, Wetting phase permeability in a partially saturated horizontal fracture, paper presented at the Fifth Annual International Conference on High Level Radioactive Waste Management, Am. Nucl. Soc., Las Vegas, Nev., 22–26 May 1994.

Nicholl, M. J., and R. J. Glass, Field Investigation of flow processes associated with infiltration into an initially dry fracture network at Fran Ridge, Yucca Mountain, Nevada: A photo essay and data summary, *SAND2002-1369*, 75 pp., Sandia Natl. Lab., Albuquerque, N. M., 2002.

Nicholl, M. J., R. J. Glass, and H. A. Nguyen, Gravity-driven fingering in unsaturated fractures, paper presented at the Third Annual International Conference on High Level Radioactive Waste Management, Am. Nucl. Soc., Las Vegas, Nev., 12–16 April 1992.

Nicholl, M. J., R. J. Glass, and H. A. Nguyen, Small-scale behavior of single gravity-driven fingers in an initially dry fracture, paper presented at the Fourth Annual International Conference on High Level Radioactive Waste Management, Am. Nucl. Soc., Las Vegas, Nev., 26–30 April 1993a.

Nicholl, M. J., R. J. Glass, and H. A. Nguyen, Wetting front instability in an initially wet unsaturated fracture, paper presented at Fourth Annual International Conference on High Level Radioactive Waste Management, Am. Nucl. Soc., Las Vegas, Nev., 26–30 April 1993b.

Nicholl, M. J., R. J. Glass, and S. W. Wheatcraft, Gravity-driven infiltration instability in initially dry nonhorizontal fractures, *Water Resour. Res.*, *30*(9), 2533–2546, 1994.

Nicholl, M. J., H. Rajaram, and R. J. Glass, Factors controlling satiated relative permeability in a partially-saturated horizontal fracture, *Geophys. Res. Lett.*, *27*(3), 393–396, 2000.

O'Hara, S. K., B. L. Parker, P. R. Jorgensen, and J. A. Cherry, Trichloroethene DNAPL flow and mass distribution in naturally fractured clay: Evidence of aperture variability, *Water Resour. Res.*, *36*(1), 135–147, 2000.

Or, D., and M. Tuller, Flow in unsaturated fractured porous media: Hydraulic conductivity of rough surfaces, *Water Resour. Res.*, *36*(5), 1165–1177, 2000.

Peters, R. R., and E. A. Klavetter, A continuum model for water movement in an unsaturated fractured rock mass, *Water Resour. Res.*, *24*(3), 416–430, 1988.

Pruess, K., and J. S. Y. Wang, Numerical modeling of isothermal and nonisothermal flow in unsaturated fractured rock—A review, in *Flow and Transport Through Unsaturated Fractured Rock*, *Geophys. Monogr. Ser.*, vol. 42, edited by D. D. Evans and T. J. Nicholson, pp. 11–22, AGU, Washington, D. C., 1987.

Ramirez, A., and W. Daily, Electrical imaging of the Large Block Test—Yucca Mountain, Nevada, *J. Appl. Geophys.*, *46*, 85–100, 2001.

Russell, C. E., J. W. Hess, and S. W. Tyler, Hydrogeologic investigation of flow in fractured tuffs, Rainier Mesa, Nevada Test Site, in *Flow and Transport Through Unsaturated Fractured Rock*, *Geophys. Monogr. Ser.*, vol. 42, edited by D. D. Evans and T. J. Nicholson, pp. 43–50, AGU, Washington, D. C., 1987.

Su, G. W., J. T. Geller, K. Pruess, and F. Wen, Experimental studies of water seepage and intermittent flow in unsaturated, rough-walled fractures, *Water Resour. Res.*, *35*(4), 1019–1037, 1999.

Throckmorton, C. K., and E. R. Verbeek, Joint networks in the Tiva Canyon and Topopah Springs tuffs of the Paintbrush Group, southwestern Nevada, *U.S. Geol. Surv. Open File Rep., 95-2*, 1995.

Tokunaga, T. K., and J. Wan, Water film flow along fracture surfaces of porous rock, *Water Resour. Res.*, *33*(6), 1287–1295, 1997.

Tokunaga, T. K., and J. Wan, Surface-zone flow along unsaturated rock fractures, *Water Resour. Res.*, *37*(2), 287–296, 2001a.

Tokunaga, T. K., and J. Wan, Approximate boundaries between different flow regimes in fractured rocks, *Water Resour. Res.*, *37*(8), 2103–2111, 2001b.

Totsche, K. U., J. Danzer, and I. Kogel-Knabner, DOM-enhanced retention of polycyclic aromatic hydrocarbons in soil miscible displacement experiments, *J. Environ. Qual.*, *26*(4), 1090–1100, 1997.

Wang, J. S. Y., and T. N. Narasimhan, Hydrologic mechanisms governing fluid flow in a partially saturated, fractured, porous medium, *Water Resour. Res.*, *21*(12), 1861–1874, 1985.

Wang, J. S. Y., and T. N. Narasimhan, Unsaturated flow in fractured porous media, in *Flow and Contaminant Transport in Fractured Rock*, edited by J. Bear, C. F. Tsang, and G. de Marsily, pp. 325–391, Academic, San Diego, Calif., 1993.

Weisbrod, N., R. Nativ, D. Ronen, and E. Adar, On the variability of fracture surfaces in unsaturated chalk, *Water Resour. Res.*, *34*(8), 1881–1887, 1998.

Weisbrod, N., R. Nativ, E. Adar, and D. Ronen, Impact of intermittent rainwater and wastewater flow on coated and uncoated fractures in chalk, *Water Resour. Res.*, *35*(11), 3211–3222, 1999.

Weisbrod, N., R. Nativ, E. Adar, D. Ronen, and A. Ben-Nun, The impact of coating and weathering on the properties of chalk fracture surfaces, *J. Geophys. Res.*, *105*(B12), 27,853–27,864, 2000a.

Weisbrod, N., R. Nativ, E. Adar, and D. Ronen, Salt accumulation and flushing in unsaturated fractures in an arid environment, *Ground Water*, *38*(3), 452–461, 2000b.

Wilder, D. G., W. Lin, S. C. Blair, T. Buscheck, R. C. Carlson, K. Lee, A. Meile, A. L. Ramirez, J. L. Wagoner, and J. Wang, Large Block Test status report, *UCRL-ID-128776*, Lawrence Livermore Natl. Lab., Univ. of Calif., Livermore, 1997.

Yang, I. C., G. W. Rattray, and P. Yu, Interpretation of chemical and isotopic data from boreholes in the unsaturated zone at Yucca Mountain, Nevada, *U.S. Geol. Surv. Water Resour. Invest. Rep., 96-4058*, 58 pp., 1996.

W. D. Daily and A. L. Ramirez, Lawrence Livermore National Laboratory, PO Box 808, Livermore, CA 94550, USA.

R. J. Glass, Flow Visualization and Processes Laboratory, Sandia National Laboratories, Albuquerque, NM 87185-0735, USA. (rjglass@sandia.gov)

M. J. Nicholl, Department of Materials, Metallurgical, Mining and Geological Engineering, University of Idaho, Moscow, ID 83844-3024, USA.